16th World Conference on Earthquake, 16WCEE 2017

Santiago Chile, January 9th to 13th 2017

Paper N° 4331 (Abstract ID)

Registration Code: S-C1464021319

INCLUSION OF SCATTERING IMPULSE RESPONSE FUNCTIONS IN GROUND MOTION CALCULATIONS

J. G. F. Crempien[(1)], R. J. Archuleta[(2)]

[(1)] *Research Scientist, Universidad de Chile and University of California, Santa Barbara, crempien@gmail.com.*
[(2)] *Professor Emeritus, University of California, Santa Barbara, ralph@ucsb.edu.*

Abstract

After response spectra, ground motion duration is an important engineering parameter that can greatly affect structural damage. Any synthetic ground motion model should capture observed metrics from past earthquakes such as response spectra and ground motion duration. Duration of ground motion is in part influenced by the magnitude of the earthquake, but primarily by the physical process of multiple scattering of body waves in the crust of the earth. At high frequencies (>1Hz), ground motion is stochastic in nature as well as non-stationary in both time and frequency. The multiple lapse time window method can estimate frequency dependent scattering loss and intrinsic absorption parameters for particular regions. In the work of [1], they estimated scattering impulse response functions (SIRF's) by inverting the parameters of coda envelopes at different frequency bands using the multiple lapse time window method. With these SIRF's, we generate synthetic scatterograms and convolve them with deterministic Green's functions to produce scattering Green's functions (SGF's). We used the UCSB method [2, 3] to simulate 50 stochastic realizations of kinematic rupture on a finite fault with the same location, magnitude and dimensions of the assumed earthquakes. We then compute ground acceleration with the SGF's for all 50 kinematic rupture scenarios. We compute spectral acceleration and ground motion duration based on the evolutionary Arias intensity for each synthetic seismogram and compare these simulations to the actual recorded ground motion for these events. The bias of duration is quite small and shows no trend with distance away from each assumed fault.

Keywords: ground motion duration, scattering, scattering impulse response functions, scattering Green's functions.

1. Introduction

The physical process of scattering greatly influences the duration of ground motion, an important ground motion intensity (GMI) measure. Efforts to use Fourier amplitude spectra as a metric for ground motion prediction equations emphasizes the need to realistically model scattering effects when computing ground motion for earthquake scenarios.

1.1 Numerical Modeling of SIRF's

With waveforms provided by modern seismic arrays during the 1960's, the degree of incoherency in the seismic signals was self-evident. Heterogeneity in the Earth was the prime suspect for the existence of coda waves as stated by [4]. The search for the underlying physical mechanism to produce coda led to the seminal paper of [5]. For single scattering they concluded that the coda is due to the backscattering of seismic waves off of heterogeneities in the Earth. Since then, many models have attempted to explain the scattering of waves at different length scales and at different times in recorded seismograms. [6] used a Monte Carlo approach to compute coda energy envelopes. They determined that the most important contribution of signal incoherence at the beginning of the seismograms and at close distances comes from forward scattering rather than backscattering. They also showed that at close distances and in the early portion of the coda envelope, the scattering process does not resemble the diffusion process (strong scattering) but that later portions of the coda envelopes are most likely due to a diffusion process. [7] produced a closed form solution for the energy envelope from multiple scattering in homogeneous scattering mediums that captures the essence of the coda, which is shown in Eq. (1).

$$E(r,t)=\frac{\delta\left(t-\frac{r}{v}\right)e^{-\eta vt}}{4\pi vr^2}+\sum_{n=1}^{2}E_n(r,t)$$
$$+\int_{-\infty}^{\infty}\frac{e^{i\Omega r}}{2\pi}d\Omega\int_{0}^{\infty}\frac{\left(\frac{\eta_s}{k}\right)^3\left[\tan^{-1}\left(\frac{k}{\eta+i\Omega/v}\right)\right]^4\sin(kr)}{2\pi^2 vr\left[1-\frac{\eta_s}{k}\tan^{-1}\left(\frac{k}{\eta+i\Omega/v}\right)\right]}dk \quad (1)$$

The total incident wave energy, E_0 is assumed to be $1/v$, and v is the shear wave velocity. E_1 and E_2 model the single and double scattering energies, r is the traveled distance, t is lapse-time, $i\Omega$ corresponds to the Fourier transform with respect to time, k is the wavenumber, r is the distance from the source to the observer, η_i and η_s are the absorption and scattering coefficients and $\eta = \eta_i + \eta_s$. The extinction length, L_e and the seismic albedo, B_0 are parameters used to describe synthetic coda envelopes, and are directly related to the absorption and scattering coefficients as $L_e = 1/\eta$ and $B_0 = \eta_s / L_e$. The seismic albedo controls the decay rate of the coda envelope in terms of lapse-time. A higher seismic albedo (stronger scattering) leads to longer coda tails.
[8] showed that Eq. (2) could be approximated with a more compact solution as:

$$E(r,t)=E_0e^{-\eta vt}\left[\frac{\delta(t-r/v)}{4\pi vr^2}+\frac{\eta_s H(t-r/v)}{4\pi vt}\ln\left(\frac{1+r/(vt)}{1-r/(vt)}\right)\right]$$
$$+cH\left(t-\frac{r}{v}\right)\left(\frac{3\eta_s}{4\pi vt}\right)^{3/2}e^{\frac{3\eta_s r^2}{4vt}-\eta_i vt} \quad (2)$$

Eq. (2) is easy to compute as opposed to Eq. (1), which makes it more attractive to use as an envelope to simulate a non-stationary synthetic coda process.

1.2 Phenomenological Observations of SIRF's

[,9] analyzed the coda of several earthquakes in California and showed that at different frequency bands, the coda energy envelopes exhibit different durations for different tectonic regions (Fig.1).

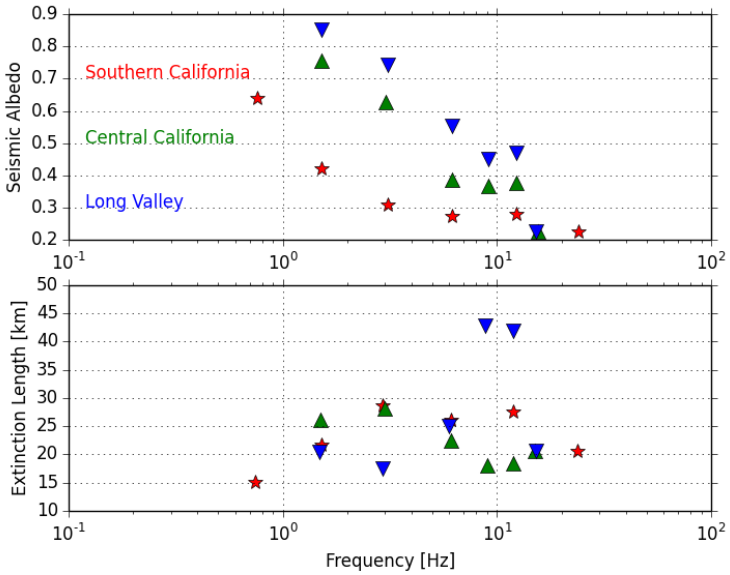

Fig. 1 – Inverted scattering parameters for different tectonic regions and frequency bands. The red stars, green triangles and blue inverted triangles correspond to the regions of Southern California, Central California and Long Valley in California (Modified from [9]).

This observation also implies that scattering can be modeled as a non-stationary stochastic process, both in time and in frequency. To see this property, we show in Fig.2 the horizontal components of acceleration from a **M**3.6 aftershock of the 2015 Napa earthquake recorded on a station ~8 km away from the fault. The difference in the temporal decay of SIRF energy density on a log scale versus time for different frequency bands is quite substantial.

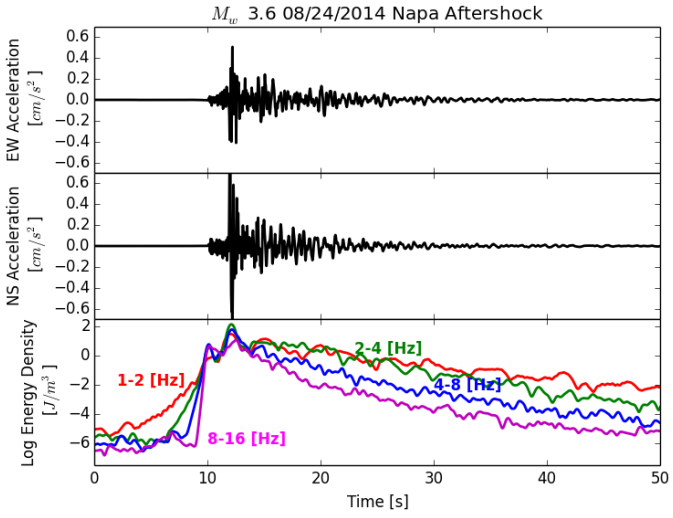

Fig. 2 – The plot shown is the recorded acceleration of a **M**3.6 Napa aftershock at ~8km. The energy density in log scale shows that at different frequency bands, scattering (the envelope decay) is quite different and therefore the duration of ground motion as well.

With the stable properties of the seismic coda, we can extract this information from a target region and incorporate the stochastic scattering process into synthetic simulations of ground motion.

2. Inclusion of Scattering in Synthetic Seismograms

Noting the non-stationarity nature of the seismic coda in time and frequency observed by [9], we use a modulating function in both frequency and time to simulate synthetic scatterograms based on [10, 11] work. We implement a discretization scheme proposed by [12, 13], such that the for each frequency band, we simulate a stationary normal distribution white noise and band-passed for each frequency band as shown in the Eq. (3) and show a schematic representation in Fig.3.

$$s(t) = \sum_{i=1}^{M} \phi_i(t) x(t) \tag{3}$$

where $\phi_i(t)$ are deterministic modulating functions for each frequency band, $x_i(t)$ are stochastic realizations of normally distributed Gaussian white noise, band-passed in the corresponding i^{th} frequency band, and M is the number of frequency bands. With the envelope functions defined by [8] to model only the S-wave scattering process, for each station-subfault pair, we later normalize these scatterograms to the FAS of the direct arrival in Zeng's equation. Once the scatterograms are constructed for each station-subfault pair, we convolve them with the corresponding Green functions and add the resultant stochastic realization to the Green's functions.

This technique preserves the main phases that are attributed to specific rays that travel within the 1D crustal model. In Fig.3 we show two Green's functions at epicentral distances of 57.3 and 87.43 km computed for a reverse fault with a 45˚ dip (r45) and a strike-slip fault (tss) at a depth of 10 km. The red curve is the actual Green's function and the black curve corresponds to the stochastic Green's functions (SGF's).

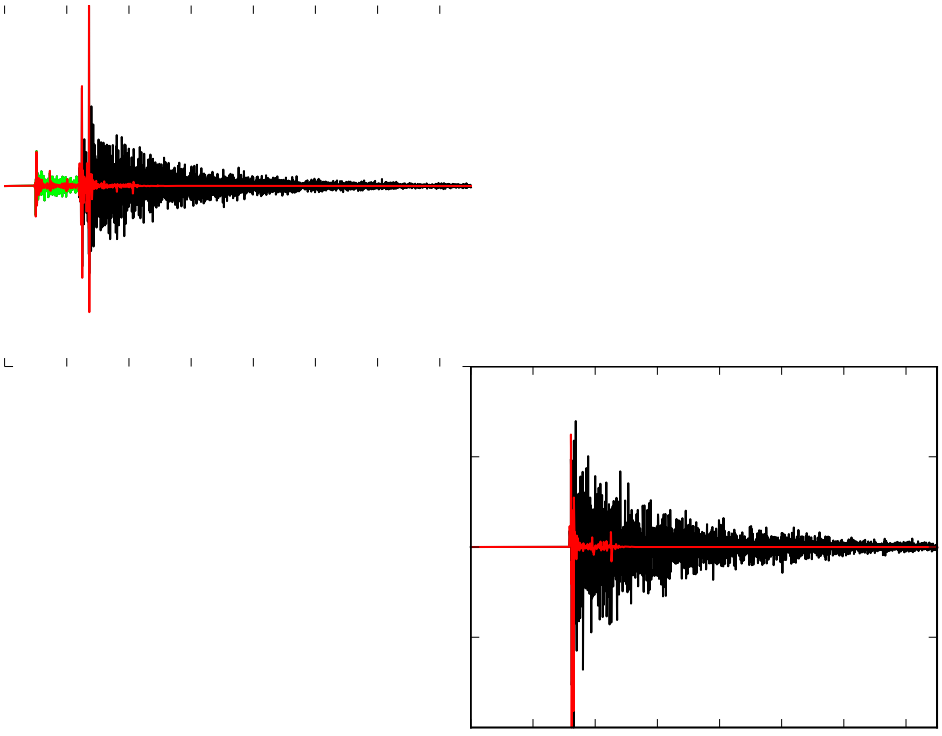

Fig. 3 – Comparison between deterministic (in solid red) and scattering (in solid black) Green's functions at different epicentral distances for r45 and tss source at a depth of 10 km. In lime we show the P-wave scattering (in solid green), which is assumed to be the same as S-waves.

We used scattering envelopes based on the seismic albedo and extinction lengths for each frequency band shown by [1, 9] for southern California. We then use the representation theorem to convolve a stochastic realization of kinematic rupture of the target earthquake with the SGF's.

Because the P-wave coda is not the main energy present in seismograms with this approach we compute synthetics for the P-waves and their respective coda assuming that the scattering process is the same as S-waves. The amplitude of this part of the seismograms, as shown in lime color in Fig.3, should not be trusted.

3. Examples

We have redone many of the earthquake rupture scenarios within southern California explained in [14] with the inclusion of scattering in our Green's functions. After several tests we have performed, we see small differences in the variability of computed ground motion of 16 realizations with respect to the original 50 realizations shown in [14].

3.1 **M**6.2 Strike Slip Earthquake Scenario

In Fig.4 we show the mean (and standard deviation) acceleration response spectra from 50 realizations of a **M** 6.2 strike-slip earthquake compared with the mean GMPE prediction. The red dots correspond to the mean of RotD50 spectra of all realizations at each period. The blue boxes are the 90% confidence intervals of the realizations and the whiskers show the maxima and minima of the realizations. The black solid line corresponds to the mean of the 2008 NGA GMPE models and the dashed line corresponds to the limits of acceptability of the synthetic ground motion for the SCEC validation exercise ([14]).

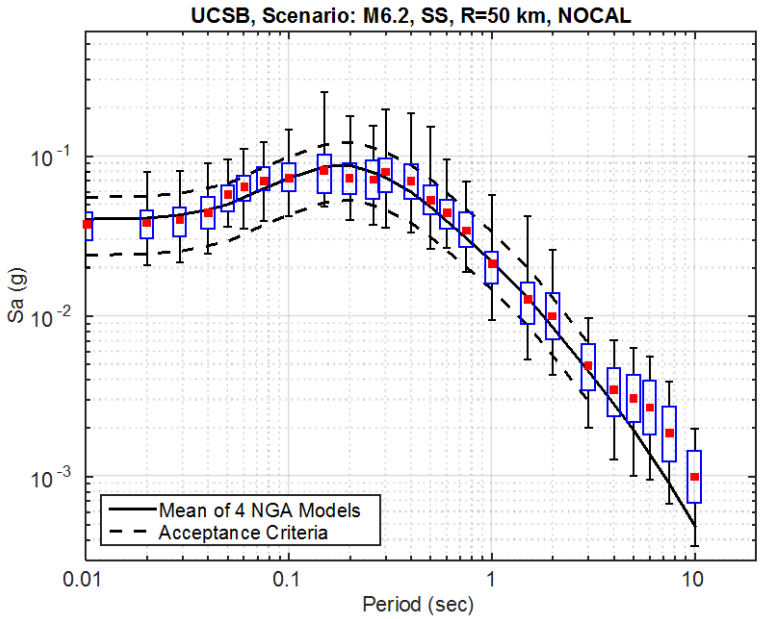

Fig. 4 – We show the statistics of 16 realizations of a **M** 6.2 strike-slip, where the median RotD50 spectrum is depicted as a red dot at each period for all stations. The blue boxes represent 90% confidence intervals of mean and the black whiskers are the extrema of the 50 simulations for all stations and realizations. The black solid line is the average of the four 2008 NGA-West1 GMPE models, as described in [14]. In all plots, results are for a set of stations at 50 km closest distance to the rupture plane.

These results show almost no variation compared with the original results of the UCSB model shown in [3]. These results capture the ground motion intensities predicted by the NGA GMPE's. We can still see higher amplitudes at the longer periods—a feature already identified by [3] as over prediction due to the use of 1D crustal structure, which naturally creates and amplifies surface waves for frequencies below 1.0-0.5 Hz.

3.2 **M**6.7 Northridge Earthquake

We have simulated ground motions at different stations that recorded the 1994 **M**6.7 Northridge earthquake. We also compute for each station an engineering parameter called RotD50, which is the median value of peak response spectra for all possible polarizations of ground motion resulting from two perpendicular recordings. When we compare our synthetic simulations to the observed ground motions, we still observe no significant differences between the RotD50 spectral amplitudes of our model with and without scattering. In Fig.5 we show results with and without scattering of the combined bias for all stochastic realizations and stations for each period. The black line corresponds to the mean bias; the magenta region is the 90% confidence interval of the mean bias; and the lavender region shows the standard deviation around the mean.

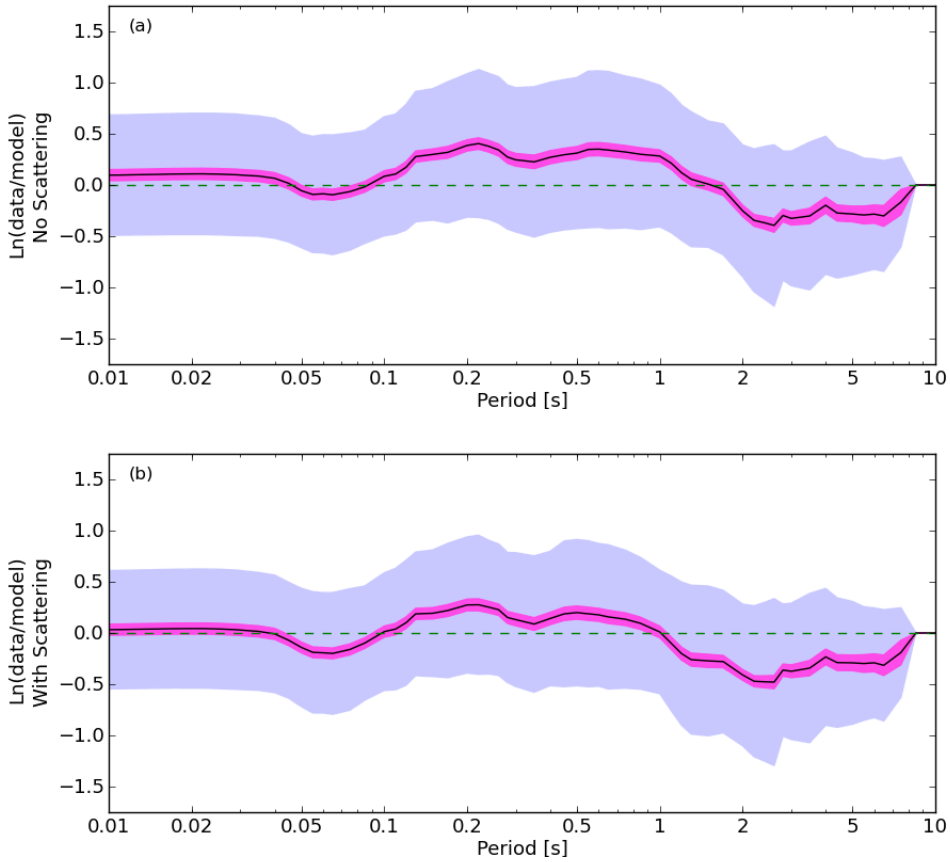

Fig. 5 – This plot shows the results of 16 realizations of bias for (a) no scattering and (b) inclusion of scattering. The black line is the mean bias, the magenta area corresponds to the 90% confidence interval of mean and the lavender region depicts the standard deviation around the mean.

These results are promising because our primary goal is to capture with our model the observed GMI's related to response spectrum. However, there are also important GMI's related to strong ground motion durations that should be captured as well by the model, specifically, the duration of ground motion based on Arias intensity. We have chosen to check the duration between 5 and 75% of the total Arias intensity (Fig.6). The original model underestimates ground motion duration by almost 0.5 in natural logarithmic scale. The model that includes scattering produces a much better estimate of Arias intensity (Fig.6b), with the exception of the furthest stations. The over-prediction at larger distances is mostly seen at stations that are in the Mojave Desert on the eastern side

of the San Gabriel Mountains. The decrease of SIRF amplitude across mountain ranges has been previously observed for *Lg* and scattered *Lg* waves (across the Alpine Range) by [15, 16].

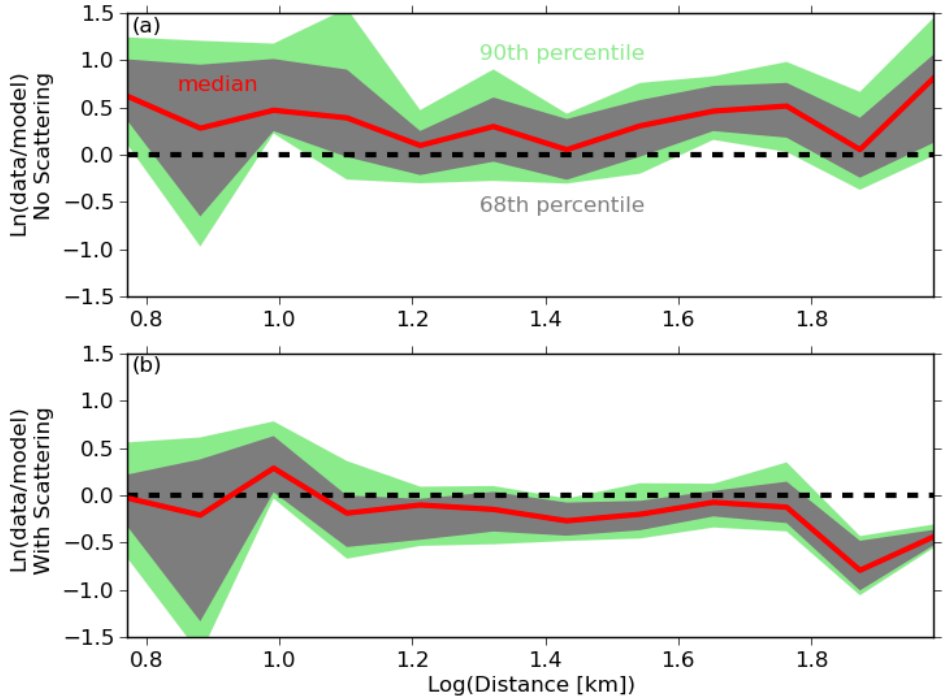

Fig. 6 – (a) and (b) show the log-bias between synthetic and observed ground motion duration without and with scattering, respectively, versus distance. The duration is based on the time between 5 and 75% of the total Arias intensity. The red line corresponds to the median of duration, the grey and light grey areas correspond to the 68th and 90th percentile respectivley. The statistics are drawn at different bins of closest distance from station to the fault and 16 realizations.

This shows some of the limitations of SIRF's determined for entire regions, without taking into consideration the azimuthal dependence or the effects of lateral crustal inhomogeneities have on SIRF amplitude decay.

4. Discussion

SIRF's determined with the method of multiple lapse-time window analysis assumes that scattering is an azimuthally independent process. Therefore, anelastic and scattering parameters of wave amplitude decay are assumed to be constant azimuthally. However, the SIRF amplitude can be quite different at different receiver points within a region for a same distance away from the source. This problem can be solved with the use of a specially tailored empirical SIRF at a specific station. With this purpose, one can turn to the original work of [17], where they construct regional coda scattering functions based on the stacking of observed SIRF's produced by earthquakes in specific segments of the scenario fault at particular stations.

5. Conclusions

We have developed a new model to simulate strong ground motion which better predicts ground motion duration. This new model incorporates the physical process of scattering. The method depends on the selection of SIRF's to characterize the envelope functions that will modulate stationary Gaussian stochastic processes to create a scatterogram. The scatterograms for different sub-source stations pairs are then convolved with Green's functions to preserve the phases of the 1D velocity structure of the region where ground motions are computed.

The new stochastic Green's functions are then convolved with the slip-rate functions at each sub-fault, and summed over the fault to produce synthetic strong ground motion at each station with the UCSB method. With this approach the UCSB model has negligible bias of RotD50 with respect to NGA GMPE's and the 1994 Northridge earthquake recordings. The bias between synthetic and observed ground motion duration is greatly improved with the inclusion of scatterograms into the Green's functions.

For regions with more complicated local geologies that show azimuthally dependent amplitudes and durations of SIRF's, we propose to use empirically derived SIRF's by stacking SIRF's produced by small magnitude earthquakes.

6. References

[1] Jin, A., K. Mayeda, D. Adams, and K. Aki (1994): Separation of intrinsic and scattering attenuation in southern California using TERRAscope data, *J. Geophys. Res.*, **99**, 17835-17848.

[2] Schmedes, J., R. J. Archuleta, and D. Lavallée (2010): Correlation of earthquake source parameters inferred from dynamic rupture simulations, *J. Geophys. Res.*, **115**, B03304, doi:10.1029/2009JB006689.

[3] Crempien, J. and R. J. Archuleta (2015): UCSB synthetic broadband ground motion method for kinematic simulations of earthquakes, *Seismol. Res. Lett.*, **86**, 1, 61-67, doi:10.1785/0220140103.

[4] Herraiz, M. and A. F. Espinosa (1987): Coda waves: A review, *Pure and Applied Geophys.*, **125**, 499-577.

[5] Aki, K., and B. Chouet (1975): Origin of coda waves, attenuation, and scattering effects, *J. Geophys. Res.*, **80**, 3322-3342.

[6] Gusev, A. A., and I. R. Abubakirov (1987): Monte-Carlo simulation of record envelope of a near earthquake. *Physics of the Earth and Planetary Interiors*, **49**, 30-36.

[7] Zeng, Y., F. Su, and K. Aki (1991): Scattered wave energy propagation in a random isotropic scattering medium, *J. Geophys. Res.*, **96**, 607-619.

[8] Zeng, Y. (1991): Compact solutions for multiple scattered wave energy in time domain, *Bull. Seismol. Soc. Am.*, **81**, 1022-1029.

[9] Mayeda, K., and W. R. Walter (1996): Moment, energy, stress drop, and source spectra of western United States earthquakes from regional coda envelopes, *J. Geophys. Res.*, **101**, 11195-11208.

[10] Priestley, M. B. (1965): Evolutionary spectra and non-stationary processes, *J. Royal Statistical Society*, **27**, 204-237.

[11] Preumont, A. (1985): The generation of non-separable artificial earthquake accelerograms for the design of nuclear power plants, *Nuclear Engineering and Design*, **88**, 59-67.

[12] Der Kiureghian, A., J. Crempien (1989). An evolutionary model for earthquake ground motion. *Structural safety*, **6** (2), 235-246.

[13] Goulet, C. A., and N. A. Abrahamson (2015): The SCEC broadband platform validation exercise for pseudo-spectral acceleration: methodology for code validation in the context of seismic hazard analyses, *Seismol. Res. Lett.*, **86**, 1, 17-26, doi:10.1785/0220140104.

[14] Campillo, M., B. Feignier, M. Bouchon, and N. Béthoux (1993): Attenuation of crustal waves across the Alpine Range, *J. Geophys. Res.*, **98**, B2, 1987-1996, doi:10.1029/92JB02357.

[15] Eva, C., M. Cattaneo, P. Augliera, and M. Pasta (1991): Regional coda Q variations in the western Alps (northern Italy), *Phys. Earth Planet. Inter.*, **67**, 76-86.

[16] Baltay, A., G. Prieto, and G. C. Beroza (2010): Radiated seismic energy from coda measurements indicates no scaling in apparent stress with seismic moment, *J. Geophys. Res.* **115**, B8, 1-12, doi:10.1029/2009JB006736.